Chapter 13

Microfluidics in CO_2 Capture, Sequestration, and Applications

Taotao Fu

Additional information is available at the end of the chapter

http://dx.doi.org/10.5772/64284

Abstract

The abnormal climate change has made the reduction of CO_2 emission that received worldwide attention. The integration of CO_2 capture-sequestration application for enhanced oil recovery (EOR) technology will be the new trend. Several scholars have applied microfluidics in CO_2 capture, oil and gas analysis, and CO_2 sequestration. The mass transfer process for CO_2 capture can be intensified owing to the large specific surface/volume ratio and high contact area in microchannels. The small amount of feeding volumes of oil and gas samples and the quick response for the analysis make the microfluidics a promising tool for the oil and gas analysis. Moreover, microfluidics can reveal the transport mechanism at microscale for multiphase interfacial phenomena in microchannels within porous media during the CO_2 flooding process in line with the pressure, temperature, and material properties of the rock within the oil reservoir. This chapter will elaborate the progress of the application of microfluidic technology in the utilization of CO_2, including the mechanism of mass transfer for CO_2 in microreactors, the advantages of microfluidics in oil and gas analysis, and the fundamentals of microfluidics in CO_2 flooding, oil recovery improvement, and CO_2 sequestration.

Keywords: CO_2, fluid dynamics, interfacial phenomena, mass transfer, microfluidics, multiphase flow

1. Introduction

1.1. Progress of the intensification and mechanism of mass transfer for CO_2 capture in microreactors

Microreactors consist of microchannels with dimensions of several hundreds of micrometers. The pressure gradient, temperature gradient, and concentration gradient augment rapidly with the decrease of the length scale in microreactors, leading to the increase of the driving forces in mass transfer and heat transfer. With the scale down to micrometers, the surface/volume ratio

is enhanced usually to 10,000–50,000 m^2/m^3 (100–1000 m^2/m^3 in conventional equipment in chemical engineering processes), which is beneficial for the intensification of mass/heat transfer. The volume of the microreactors is significantly reduced also with the decrease of the length scale. Furthermore, the numbering-up strategy for the scale-up of microreactors is beneficial for the reactions with heat and explosion. The product properties can also be improved: strengthening of the transfer process can effectively improve the conversion, selectivity, and conversion rate of the product in the microreaction system. In addition, the microreactor is beneficial for the preparation of polymer particles, microcapsule and microemulsions due to the well-controlled property of the formation, structure, and composition of the polymer and the multiphase systems by using microreactors [1, 2]. The mass transfer process for CO_2 capture in microreactors is associated with the interfacial surface area between the CO_2 and the flowing liquid, contact method, reactor type and geometry, and flowing conditions as well as the liquid and gas properties [3]. Slug flow is found to be the most widely used flow pattern for CO_2 in flowing liquids in microchannels among other flow patterns such as bubbly flow, annular flow, and parallel flow. This section will review the fluid dynamics for gas-liquid two-phase flow in microchannels and the mass transfer mechanism for CO_2 capture in microreactors.

1.2. Pressure drop for gas-liquid two-phase flow in microchannels

The characteristics for the pressure for gas-liquid two-phase flow in microchannels differ significantly from those in conventional large-scale pipes due to the predominated effects of surface tension forces and viscous forces at the microscale in microchannels. The prediction for the pressure drop for gas-liquid two-phase flow in microchannels includes physical model, Lockhart-Martinelli model, and homogeneous model.

The pressure drop in the liquid filled microchannels with slug bubbles ΔP includes ΔP_B along the slug bubble induced by the frictional loss in the liquid film between the bubble and the channel walls, ΔP_{Caps} induced by the Laplace pressure across the caps of slug bubbles, and ΔP_F in the liquid plug. The pressure drop induced by the frictional loss in the liquid film and gutters between the bubble and the channel walls is often neglected in comparison with the other two kinds of pressure drops, both for bubbles in surfactant-free liquids and for the liquid phase with surfactants whose concentration is high enough [4, 5]. However, for intermediate concentrations of surfactant in the liquid, the pressure decreases rapidly across the body of the bubble owing to the concentration gradient of surfactant along the interface, giving rise to tangential surface tension tractions to immobilize the interface. This would increase the pressure drop across the bubble. Thus, bubbles within the channel can induce additional resistance to the flow, and the pressure drop across a single bubble within the microchannel ΔP_B can be evaluated by using Bretherton expression [6] and Ratulowski and Chang [7] expression, by assuming that Bretherton's law is valid in square and circular cross-section:

$$\Delta P_B = \begin{cases} 3.58\dfrac{\sigma}{r}\left(\dfrac{3\mu u}{\sigma}\right)^{2/3} & \text{Ca} \le 10^{-2} \\ 3.58\dfrac{\sigma}{r}\left(\dfrac{3\mu u}{\sigma}\right)^{2/3} - 9.07\dfrac{\sigma}{r}\left(\dfrac{3\mu u}{\sigma}\right)^{0.95} & 10^{-2} \le \text{Ca} \le 10^{-1} \end{cases} \quad (1)$$

http://dx.doi.org/10.5772/64284

where μ is the liquid viscosity, u is the superficial velocity of the gas-liquid flow, σ is the surface tension between the liquid and gas phases, and r is the radius of the microchannel. Whereas the whole Laplace pressure across bubbles in microchannels is related to the number of bubbles, which is hard to obtain in industrial processes. Thus, the whole Laplace pressure is always estimated by modifying the frictional factor for the pressure drop for single liquid-filled microchannel.

The frictional pressure between the liquid plug and the channel wall can be estimated by using the Hagen-Poiseuille equation at low Reynolds numbers, in which case the fluid flow in the liquid slug is deemed as laminar flow [8]:

$$\Delta P_F = f\left(\frac{4}{d_{\mathrm{H}}}\right)\left(\frac{1}{2}\rho u^2\right)\left(L_{\mathrm{S}}\right) \tag{2}$$

where d_{H} is the equivalent diameter of the microchanel, ρ is the liquid density, and L_{S} is the length of the liquid plug. It should be pointed out that the pressure drop for gas-liquid two-phase flow in the slug bubble flow in microchannels is therefore related to the size and number of bubbles, which can modify the occupation for each part of pressure in the whole pressure drop in microchannels. However, for bubbles flowing in fluids in nontransparent microchannels during the application, the prediction of pressure drop for gas-liquid two-phase flow becomes difficult by using the physical model, as the lengths of the bubbles and liquid plugs are hard to obtain directly. It should be noted that the volume of a bubble flowing through a microchannel can be varied with the reduction of pressure along the channel. This effect becomes more pronounced in long microchannels. Moreover, the pressure drop of bubbles flowing in fluid-filled microchannels is also affected by the cross-section of the channel. Ratulowski and Chang [7] established an empirical expression to relate the pressure drop across a bubble and the capillary number in a square cross-sectional microchannel as $\Delta P_B = 12.2\mathrm{Ca}^{0.55}$, when $3 \times 10^{-3} < \mathrm{Ca} < 0.1$ [7, 9]. Wong et al. [10] extended Bretherton's analysis [6] to rectangular microchannels: $\Delta P_B \sim \sigma / r \sim \mathrm{Ca}^{2/3}$. However, the analysis by Wong et al. [10] does not provide an explicit function form for $\Delta P_B \sim \sigma \mathrm{Ca}^{2/3} / r$. Ca ($\mathrm{Ca} = \mu u / \sigma$) is the capillary number, representing the ratio of the relative viscous force to surface tension force.

Lockhart and Martinelli proposed the prediction for gas-liquid two-phase flow in microchannels related to the pressure for a single liquid-filled microchannel by using a friction multiplier of the liquid phase, which can be expressed by the gas and liquid viscosity and density, and the volumetric fraction of the gas phase. In the homogeneous model, the gas and liquid phases are deemed to be mixed uniformly in microchannels. This model is proposed to predict the pressure drop for gas-liquid two-phase flow in conventional channels, with the prerequisite that the gas and liquid phases are mixed uniformly, i.e., the gas phase is dispersed uniformly in the liquid in the form of very tiny bubbles. However, in microchannels, this regime can only be achieved at extreme conditions. That is to say, this model is not valid in most situations in microfluidics applications.

1.3. Mass transfer of gas-liquid two-phase flow in microchannels

1.3.1. Mass transfer of gas-liquid two-phase flow under various flow patterns

The mass transfer between gas and liquid phases in microchannels dominates the flow patterns, which usually contain bubbly flow, slug flow, churn flow, annular flow, and parallel flow.

1.3.1.1. Bubbly flow

In this flow pattern, the diameter of bubbles is less than the channel diameter, which usually occurs under low superficial velocity of the gas phase and high superficial velocity of the liquid phase. The diameter of bubbles is manipulated by the gas and liquid flow rates, physical property of the fluids, and how two phases contact. In general, the surface area between gas and liquid phases increases with the reduction of the bubble size, which is beneficial for the enhancement of the mass transfer process.

1.3.1.2. Churn flow

Churn flow happens at high superficial velocity of the gas phase, within which long gas slugs and short liquid plugs pass through the channel. It is found that the mass transfer coefficient is higher in the churn flow than that in the slug flow. Yue et al. [11] found that the mass transfer coefficient increases with the increase of the gas flow rates and liquid flow rates.

1.3.1.3. Annular flow and parallel flow

When the superficial velocity of the gas phase is relatively high and that of the liquid phase is quite low, annular flow and parallel flow occurs, depending on the geometry of the contactor for the two-phase flows. The former is likely to happen at flow-focusing junctions, while the latter for T- and Y-junctions usually. In both cases, the gas and liquid streams flow in parallel along the microchannel, and the mass transfer thereby occurs at the interface of the gas-liquid two-phase flow. The experimental results show that in falling film microreactors, the enhancement of the mass transfer rate in the CO_2-monoethanolamine-H_2O system can be obtained [12]. However, the Marangoni effect in the falling film microreactor seems to be weaker than that in macrosystems, signifying that the convection partially prevented by the limited size of the microchannel [12].

1.3.1.4. Slug flow

The mass transfer for slug flow in the gas-liquid two-phase flow in microchannels depends on the flow conditions, physical property of the fluids, the hydrodynamics of the fluids, and the geometry of microchannels. As this flow regime is always achieved at most of microfluidic applications, the following section will mainly focus on this flow regime.

1.3.2. Mass transfer mechanism

The key issue for mass transfer mechanism for gas-liquid two-phase flow in microchannels is to reveal the mass transfer rule across the gas-liquid interface and the influence of the lengths

of the gas slug and liquid plug on the mass transfer coefficient. Bercic et al. [13] investigated the absorption of CH_4 by using water in capillaries with diameters ranging from 1.5 to 3.1 mm, and found that the volumetric mass transfer coefficient $k_L a$ is predominated by the length of plugs rather than the length of bubbles when the liquid plugs are sufficient long. In their experiments, the mass transfer around the caps of the slugs dominates the whole process, and the mass transfer coefficient is proposed as

$$k_L a = \frac{0.111u^{1.19}}{\left(\left(1-\varepsilon_G\right)\left(L_B + L_S\right)\right)^{0.57}} \tag{3}$$

where L_B, L_S are, respectively, the length of the bubble and liquid plug. Van Baten et al. [14, 15] divided the mass transfer coefficient $k_L a$ for mass transport process for slug bubbles to the liquid plugs in vertical capillaries into two parts: one between bubbles' caps and plugs $k_{L,\,cap}a_{cap}$, and the other one between cylindrical parts of slug bubbles and the liquid films between the bubble and walls $k_{L,film}a_{film}$:

$$k_L a = k_{L,film}a_{film} + k_{L,\,cap}a_{cap} \tag{4}$$

When $Fo<0.1$, both parts for the mass transfer process are important. When $Fo>0.1$, the liquid films are saturated and the mass transfer between the caps and liquid plugs predominates. The liquid side mass transfer coefficient in the film can be calculated as

$$k_{L,film} = 2\sqrt{\frac{D}{\pi t_{film}}}\frac{\ln\left(1/\Delta\right)}{1-\Delta};(Fo<0.1),\ \text{and} \tag{5}$$

$$k_{L,film} = 3.14\frac{D}{\delta_{film}};\ (Fo>0.1) \tag{6}$$

where $(Fo=\frac{D}{t_{film}\delta^2_{film}})$, D is the diffusivity coefficient, and δ_{film} is the film thickness $t_{film}=\frac{L_{film}}{U_B}\approx\frac{L_B-d_h}{U_B}$. Vandu et al. [16] found deviation between the experimental results and the predictions by using the expression proposed by van Baten et al. [14] for the absorption process of O_2 in water. They deemed that the deviation was caused by the fact that the van Baten et al.'s expression validated for long mass transfer unit, in which situation the liquid film between the bubble and the channel walls is saturated; while in the experiments of Vandu et al. [16], the length of the liquid film is short and the velocity of the bubble is high to make the liquid film unsaturated. Vandu et al. [16] obtained the mass transfer coefficient for the bubble caps

by using the classical penetration theory for mass transfer process as: $k_{\mathrm{L,cap}}a_{\mathrm{cap}}=2\frac{\sqrt{2}}{\pi}\sqrt{\frac{DU_{\mathrm{B}}}{d_h}}$. Mass transfer coefficient for the liquid film by using the unsteady diffusion model as $k_{\mathrm{L,film}}a_{\mathrm{film}}=2\sqrt{\frac{DU_{\mathrm{B}}}{\pi t_{\mathrm{film}}}}$

$$k_{\mathrm{L}}a=\frac{2}{\sqrt{\pi}}\sqrt{\frac{DU_{\mathrm{B}}}{\left(L_{\mathrm{B}}-d_h\right)}}\frac{4\left(L_{\mathrm{B}}-d_h\right)}{dh\left(L_{\mathrm{B}}+L_{\mathrm{S}}\right)}+2\frac{\sqrt{2}}{\pi}\sqrt{\frac{DU_{\mathrm{B}}}{d_h}}\frac{4}{L_{\mathrm{B}}+L_{\mathrm{S}}} \tag{7}$$

This equation is available for the situation when the mass transfer in the liquid film is predominated and unsaturated at $(u/L_{\mathrm{S}})^{0.5}>3\mathrm{s}^{-0.5}$. Another experimental fitting proposed by Yue et al. [17] is illustrated as $k_{\mathrm{L}}a=2(DU_{\mathrm{B}}/(L_{\mathrm{B}}+L_{\mathrm{S}}))^{0.5}(L_{\mathrm{B}}/(L_{\mathrm{B}}+L_{\mathrm{S}}))^{0.3}\cdot d_{\mathrm{H}}{}^{-1}$ by performing experiments for the absorption of O_2 in water in square microchannels. The experiments of Yue et al. [17] were operated under short film contact time so that the mixing between the liquid film and the liquid plug is poor. In this case, the predictions proposed by van Baten et al. [14] and Vandu et al. [16] are not applicable. It is noteworthy that these expressions are applicable for physical absorptions process with tiny mass transfer between gas and liquid phases, in which the characteristic parameters for bubble slugs and liquid plugs should be evaluated to obtain the mass transfer coefficient. This limits the applications of these predictions. Furthermore, Yue et al. [17] suggested that the quantitative information on the circulation in liquid plugs and the mixing between the liquid film and liquid plug needs to be revealed for constructing a universal model for mass transfer in bubble slug flow pattern for the gas-liquid two-phase flow in microchannels.

For practical application several predictions for the mass transfer coefficient were proposed by using either the nondimensional analysis or energy dissipative model. Yue et al. [11] correlated the mass transfer coefficient in the form of the Sherwood number *Sh* with the Schmidt number *Sc* (representing the physical property of the fluids) and the Reynolds number *Re* (representing the flow conditions) as $Sh_L\cdot a\cdot d_h=0.084\mathrm{Re}_G^{0.213}\mathrm{Re}_L^{0.937}Sc_L^{0.5}$ for slug flow for the physical absorption of CO_2 into water in rectangular microchannels. Sh_{L} is the liquid Sherwood number defined by $Sh_L=k_{\mathrm{L}}d_h/D_{\mathrm{CO2}}$, representing the relative magnitude of the liquid side mass transfer coefficient k_{L} to the diffusivity of CO_2 in the liquid. Sc_{L} is the liquid Schmidt number defined by $Sc_L=\mu_L/\rho_L D_{\mathrm{CO2}}$, representing the relative magnitude of the momentum diffusivity to the mass diffusivity. Re_G and Re_L are respectively the Reynolds number of the gas and liquid phases, defined by $\mathrm{Re}=\rho u d_h/\mu$, representing the relative magnitude of the inertial forces to the viscous forces. These methods provide experimentally and semitheoretically the mass transfer coefficient prediction with relatively high precision only if the applications are conducted within the range of the experimental conditions performed by Yue et al. [11]. However, this method needs a series of experiments in a wide range.

The energy dissipative model [18] correlates the mass transfer coefficient with the dissipative parameter ς (defined as $\varsigma=\left(\frac{\Delta p_F}{L}\right)_{TP}u$) as the pressure drop along the channel differs for the

gas-liquid two-phase flow with and without mass transfer [18]. Δp_F is the two-phase frictional pressure drop, L is the length of the microchannel, and u is the superficial velocity. The subscript TP represents the two-phase flow. Yue et al. [11] applied this function in mass transfer for the absorption of CO_2 in water in microchannels and proposed a similar expression as $k_L a = 0.0863\left(\frac{\Delta P_F}{L}\right)_{TP}^{0.881}$ performs well for the relatively small mass transfer rates, in which situation the mass transfer process has little effect on the flow dynamics of the gas-liquid two-phase flow in microchannels. In addition, the frictional pressure drop needs to be obtained for predicting the mass transfer coefficient in this method, limiting its usage.

1.3.3. Effects on the mass transfer process

Several studies have been performed for the various effects on the mass transfer process in microchannels. Eskin et al. [19] did experiments to study the effects of the size and length of microchannels on the mass transfer process for gas-liquid two-phase flow in microchannels, and found that the mass transfer coefficient increases with the reduction of the cross-sectional radius of microchannels. They proposed a model to predict the mass transfer coefficient for the mass transfer process of slug bubbles with the liquid plugs in long microchannels by taking into account the dynamical flow hydrodynamics such as pressure drop, variation of bubble size, and the variation of the local velocities. Shao et al. [20] conducted experiments on mass transfer process of CO_2/N_2 in 0.2 M NaOH aqueous solutions and water, respectively, in 0.25–1 mm capillaries, and found that the volumetric mass transfer coefficient for the chemical absorption process is 3–12 times compared to the physical absorption process. They also studied the effects of the length of slug bubbles and liquid plugs, the velocity of bubbles, and the size of microchannels on the mass transfer process, and found that the volumetric mass transfer coefficient ranged between 0.3 and 0.5 s^{-1}. Sobieszuk et al. [21] measured the interfacial area in the slug flow in a microchannel by using the Danckwerts' method for the CO_2 absorption from CO_2/N_2 mixture into $KHCO_3/K_2CO_3$ buffer solutions, and provides, for the first time, the mass transfer coefficients separately for the liquid film and the liquid caps. Sobieszuk et al. [12] further found that the enhancement of the overall rate of the mass transfer depends on the gas concentrations. Ichiyanagi et al. [22] performed detailed three-dimensional measurements of the velocity and concentration distributions for CO_2 dissolution process through the gas-liquid interface in microchannels by using the advanced technique confocal micron-resolution particle image velocimetry (micro-PIV) combined with laser-induced fluorescence (LIF). The LIF measurement demonstrated that the dissolved gas in the spanwise direction decreases with the increase of the Reynolds number. The molar fluxes in the streamwise direction were at least 20 times compared to those in the spanwise and depthwise directions, signifying that the enhancement of the momentum transport in the spanwise and depthwise directions plays an important role in the enhancement of the mass transfer for gas-liquid slug flow in microchannels.

Several investigations have been carried out on the dynamical mass transfer process for slug bubbles for gas-liquid two-phase flow in microchannels by taking advantage of the real-time recording of the movement of bubbles in microchannels with the help of high-speed digital

camera [23-28]. Tan et al. [23] found that bubbles formed during the mass transfer process of a CO_2/N_2 mixture with contact with the NaOH aqueous solution at the microfluidic T-junction are smaller than those formed without mass transfer process. The typical time for bubble formation ranges between 0.2 and 0.4s, during which the amount of mass transfer contributes to around 30–40% of the total transferred solute. The overall mass transfer coefficient during bubble formation stage is in the range of 1.4×10^{-4} to 5.5×10^{-4} m/s, and it increases with the elevation of the gas and liquid flow rates. It is deemed that the resistance in the gas side during the mass transfer process predominates; and the circulation in the slug bubbles significantly intensifies the mass transfer with the enhancement factor in the range of 5–15. Furthermore, they studied the effects of the angle of the junction on the mass transfer coefficient and found that the mass transfer coefficient in the liquid size achieves its maximum at 90° junction, and reaches its minimum at 150° junction.

1.3.4. Intensification of the mass transfer process

In order to intensify the mass transfer of CO_2 in fluids in microreactors, several methods have been employed, such as inducing turbulence by using the third inert gas and obstacles or particles in channels, specific geometry (curved) of the channel, and active forces. Su et al. [29] found that the mass transfer process can be intensified by adding solid particles in microchannels. Su et al. [30] introduced the third phase-inert gas into the liquid-liquid two-phase flow in microchannels to enhance the mass transfer coefficient. Tan et al. [24] performed experiments to study the effects of the curvature of the curved geometry for microchannels on the absorption of CO_2 for a CO_2/N_2 mixture contacting with NaOH aqueous solution, and found that the mass transfer coefficient is greatly augmented with the decrease of the curvature radius. That is, k_L in curved channels with the curve radius of 3 cm is nearly two times compared to that in a straight channel. They also proposed an expression to predict the mass transfer coefficient as $k_{L,R}/k_{L,R\to\infty} = 1 + 91 d_H/R$, where $k_{L,R}$ and $k_{L,R\to\infty}$ are respectively the overall mass transfer coefficient in the curved channel with curve radius of R and in a straight channel, and d_H is the hydrodynamic radius of the microchannel.

The mechanism for mass transfer during CO_2 bubbles flowing in microchannels needs to be explored to be manipulated according to various applications, especially more attention should be paid to the dynamics of the gas-liquid interface during the mass transfer process and provide solid foundations for the coupling of transport and reaction, scale-up, and optimization of microreactors.

2. Microfluidic technology in oil and gas analysis, and CO_2 applications

Recently, microfluidic technique is found to be a promising tool for the oil and gas analysis, for measurements of parameters such as Henry's coefficient, solubility of gas in the liquid phase, and the gas-liquid reaction coefficient [31]. Sell et al. [32] provided a microfluidics technique to measure the diffusion coefficient for CO_2 in water and brine, with the advantage of only microliters of sample and analysis within minutes (Figure 1). However, established

macroscale pressure-volume-temperature cell methods require large sample volumes, which is completed within hours or days. They also found that pressure had no significant effect on diffusion rates, supporting an assumption applied by many sequestration models. Namely, time scales for dissolution are independent of reservoir depth or *ex situ* carbonation pressures. Fadaei et al. [33] also provided a microfluidic method to rapidly measure the CO_2 diffusivity in Bitumen, with the range of pressures of 1–5 MPa and at a room temperature of 21°C. They obtained the diffusion coefficients in the order of 10^{-10} m^2/s, agreeing well with the relevant published data using conventional methods. Compared to the traditional methods (with 0.5 L of sample within hours or days), this method requires only 10 minutes and 1 nL plug of sample.

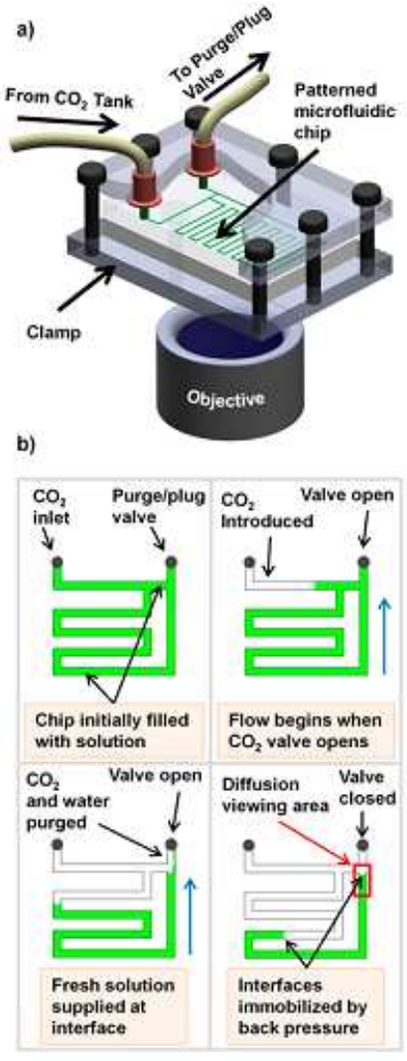

Figure 1. Microfluidic system used to measure the CO_2 diffusion coefficients in water. (a) Illustration of the experimental setup. (b) Schematic of the CO_2 diffusivity test initialization procedure. "Reprinted (adapted) with permission from Sell, A., Fadaei, H., Kim, M., Sinton, D., 2013. Measurement of CO_2 diffusivity for carbon sequestration: a microfluidic approach for reservoir-specific analysis. Environmental Science & Technology 47, 71–78. Copyright (2013) American Chemical Society." (Sell et al. [32]) http://dx.doi.org/10.1021/es303319q

Lefortier et al. [34] presented a high-throughput method to rapidly measure the diffusion coefficients and solubility of CO_2 in pure solvents and mixtures in realtime by taking advantage of the visualization of the variation of CO_2 absorption fluids in microchannels. Sun and Cubaud [25] experimentally study the dissolution of CO_2 into water, ethanol, and methanol by using the microfluidic technique (Figure 2), and found that the bubble dissolution rate depends on the inlet gas pressure and fluid pair composition. For short period of time after the contact of fluids, the bubble length decreases linearly with time, displaying a fast diffusive behavior owing to the CO_2 concentration gradient localized in the thin gas-liquid interfacial region. The initial rate of the diminishing bubble size is proportional to the ratio of the diffusion coefficient to the Henry's law constant. This study shows that the gas saturation and sequestration processes can be achieved rapidly across quite short distances in microfluidic devices.

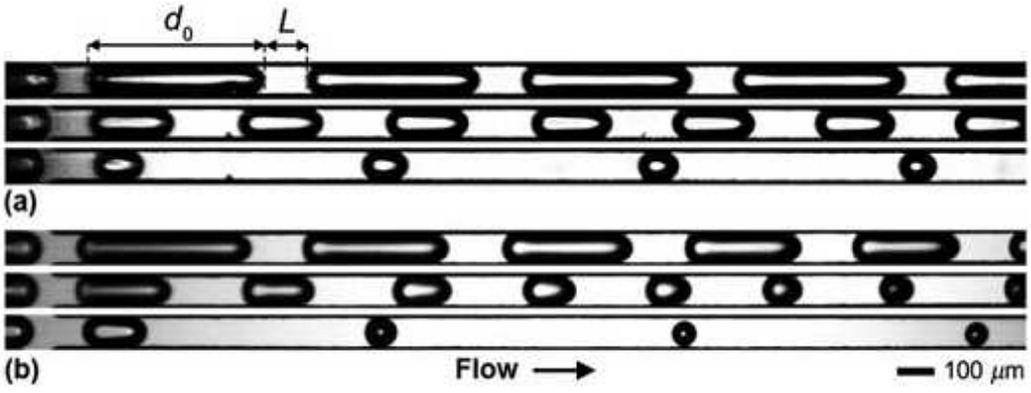

Figure 2. Examples of diffusive multiphase flows. (a) Weakly diffusive bubbles for CO_2 in water. The ratio of the liquid volumetric flow rates to the sum of the gas and liquid flow rates is 0.23, 0.47, and 0.80 from top to bottom. (b) Strong diffusive bubbles for CO_2 in methanol. The ratio of the liquid volumetric flow rates to the sum of the gas and liquid flow rates is 0.24, 0.51, and 0.68 from top to bottom. Reproduced from Sun and Cubaud [25] with permission of The Royal Society of Chemistry. http://dx.doi.org/10.1039/C1LC20348G

Abolhasani et al. [35] studied the automated microfluidic method for the rapid measurement of CO_2 mass transfer and solubility in physical solvents. The variation of slug bubbles flowing along the microchannel was dynamically recorded and analyzed to obtain the solubility of CO_2 in solvent. For CO_2-dimethyl carbonate (DMC) system, the volumetric mass transfer coefficients ranged between 4 and 30 s^{-1}, and Henry's constants were within the range of 6–12 MPa. Li et al. [36] presented a microfluidic method to study rapid gas-liquid reactions for the rapid acquisition of the kinetic data for the reaction by also capturing the dynamical variation of slug bubbles flowing in microchannels (Figure 3). In this work, the application of microfluidic method was utilized for systems with relatively low concentrations of the reagents and products and for the low-viscosity media. This method is expected to apply for the CO_2 sequestration in the oil industry. Tumarkin et al. [37] conducted similar experiments to manipulate the solubility of CO_2 in water and a 0.7 M NaCl aqueous solution, by controlling the temperature of the fluids flowing in the microchannel. Bubbles experience shrinkage-expansion-shrinkage stage, termed as "bubble breathing," when the cooling-heating-cooling system is applied to the bubble flowing system. Tumarkin et al. [38] controlled the size of

CO_2 bubbles by manipulating the temperature of the fluids, and functional particles were loaded at the gas-liquid interface to stabilize the bubble from coalescence. Park et al. [39] produced small CO_2 bubbles with a diameter less than 8 μm in microfluidic devices by manipulating the pH value of the liquid phase, and found that the bubble size depends on the flow rates of the liquid phase and the acid-base equilibrium established in the microchannels.

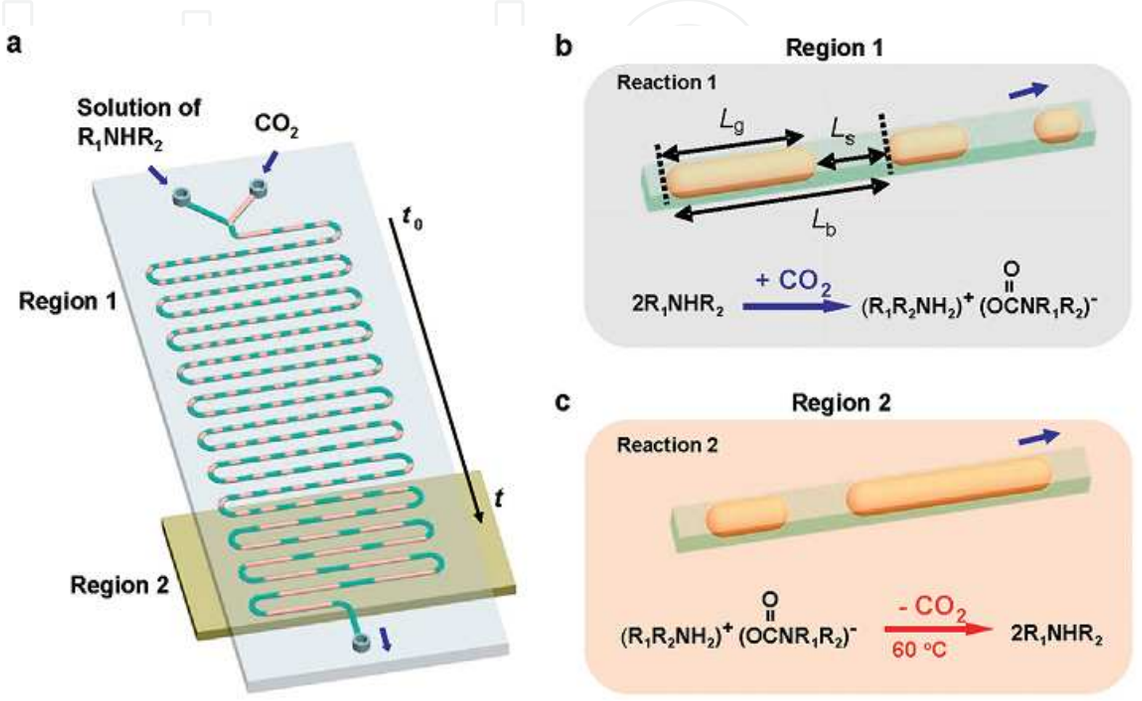

Figure 3. Reversible CO_2 binding to secondary amines performed in the microfluidic reactor. An ITO glass-based heater is placed underneath region 2, and an aluminum plate is placed underneath region 1 to maintain the temperature in this region at 23°C. (b) Reaction of CO_2 with a secondary amine in reaction 1, and the volume of CO_2 slugs decreases with CO_2 reacts with R1NHR2. (c) Release of CO_2 manipulated by the increase of the temperature in reaction 2. "Reprinted with permission from Li, W., Liu, K., Simms, R., Greener, J., Jagadeesan, D., Pinto, S., Gunther, A., Kumacheva, E., 2012. Microfluidic study of fast gas-liquid reactions. Journal of the American Chemical Society 134, 3127–3132. Copyright (2012) American Chemical Society." (Li et al. [36]) http://dx.doi.org/10.1021/ja2101278

In summary, the microfluidic technique is a promising tool toward the measurement of the physical property of fluids involved during the CO_2 application, and gas and oil analysis, with the advantage of small sample size and short analysis time. However, the dynamics and mechanisms of the fluid flow and mass transfer in microchannels needs to be highlighted to meet these applications.

3. Microfluidic technology in CO_2 flooding, improving the oil recovery and CO_2 sequestration

With the increasing concern on environmental protection, the integration of CO_2 capture-sequestration-application for enhanced oil recovery technology will be the new trend in the

future. Microfluidics technology, with the unique advantages in realtime visualization and quantification, can reveal the transport mechanism in the microscale for multiphase interfacial phenomena in microchannels within porous media during the CO_2 capture-sequestration-application in line with the pressure, temperature, and material properties of the rock within the oil reservoir. These wells or salt sand underground aquifers comprise of porous media made of many tens of microchannels in a network structure, which are consistent with the conventional scale of microchannels used in the microfluidic technique [31].

3.1. Fluid dynamics

When $CO_2$is injected into underneath wells, it becomes a supercritical fluid at the underground temperature and pressure. It is lighter than oil or brine and denser than CO_2 that is under normal conditions. Driven by the pressure, superficial CO_2 flows through the liquid-filled microchannel networks in the rock layer of porous media, and its flow paths are influenced by the heterogeneous structure of the porous media [40]. In microchannels, the tongue of CO_2 gaseous thread can breakup into bubbles driven by the capillary instability, and the generated bubbles can be captured or move through a straight microchannel or bifurcation junctions. Of course, these CO_2 bubbles will be absorbed slowly by the liquid phase [41]. In a CO_2 injection process, it usually takes three or four decades or even centuries of time for the complete absorption of CO_2. Although the microfluidic technology has been applied to study the CO_2 flooding in recent years, these studies on the dynamics and mechanics of multiphase flow in porous media consisting of microchannel networks have been carried out in the mid-20th century by the fluid mechanics community [42, 43]. For example, the famous viscous fingering phenomenon for miscible and immiscible two-phase flow in Hele-Shaw cells (rectilinear flow or radial source flow) has attracted attention for many years including the stability and nonstability mechanism of the interface, the bubble capture and release mechanism, the rupture of the interface, and the tip streaming of droplets and bubbles [44]. The interfacial phenomenon in the basic unit of the porous media network, or the loops of microchannels, has also been explored including the interfacial stability in symmetric and asymmetric loops and bubble capture in asymmetric loops [45-48]. For example, Oxaal et al. [45] studied the displacement of a high-viscosity fluid by a low-viscosity fluid that results in viscous fingering in homogeneous porous media. They found that the interfacial dynamics was dominated by the viscous forces at high flow rates and by capillary forces at low flow rates. Lenormand et al. [49] proposed a leaking mechanism to explain the dynamic phenomena in drainage for the displacement of one fluid by another in a network consisting of many ducts. They found that the wetting fluid motion at the edges was much slower than the nonwetting fluid, which was affected by the viscosity of the latter fluid. The local phenomenon was found to be linked with the drainage pressure and imbibition pressures at the microscale, and the macroscopic effect at the network scale was found to be related to the topology of the nonwetting fluid at the end of the drainage. The dynamics of trapped bubbles was influenced by their size and topology.

Recently, with the development of microfluidic techniques, detailed information on the two-phase interfacial phenomena in microfluidic loops has been explored. Al-Housseiny et al. [48]

provided a microfluidic tool to control the interfacial instability by changing the geometry of the device, and found that a gradient in the passage can lead to different displacement behaviors. This finding can be used to manipulate instabilities in fluid-fluid systems in microfluidic devices. The interesting and complex problem is that the fluid can penetrate evenly or not the two identical daughter channels in a network composed of two identical channels that are linearly vary in radius [46, 47]. When the surface tension predominates at low capillary numbers, this geometry can lead to the fluid to enter only one of the two branches, signifying that the uniform fluid penetration into the network is not always stable. At high capillary number Ca, the interface advances together and the fluid penetration is stable as viscous forces are dominant. The system can also exhibit an interplay between viscous and surface tension effects. In addition, the preferential flow penetration increases with the decrease of the viscosity ratio. This study suggested that the sweep efficiency could be enhanced if the channels in the network became narrower in the flow direction for flushing wetting oils by a low viscosity solvent. They also showed that the presence of an elastic boundary could lead to the suppression of the instability of the dynamics of the propagating gas-liquid interface for the Hele-Shaw displacement of a viscous liquid by a gas underneath an elastic membrane, governed by the surface tension at the gas-liquid interface due to the tapered flow geometry underneath the deflected membrane [50]. Controlling instability of fingers for fluid-fluid interface is fundamental to a wide range of applications such as flows in porous media in enhanced oil recovery processes and carbon sequestration [47]. Other examples of two-phase flows in spatially varying geometries are flows of bubbles and drops through junctions, constricted capillaries, flexible tubes, and tapered channels [4, 41, 51-53]. Bubbles and droplets can pass through, be captured, stay or leave, and even break up into small ones in spatially varying geometries. For example, bubbles can be trapped or released from a linear pore, governed by a capillary number [41]. The critical capillary number characteristic of the transition between trapping and releasing depends nonmonotonically on the bubble size. To better explore the dynamics of the gas-liquid interface in microchannels, the detailed flow-field distribution can be provided by advanced measurement methods, such as micro-PIV (Figure 4) [4].

3.2. Oil recovery

Haas et al. [54] presented a lab-on-a-chip method to inform oil recovery by injecting steam underground in a process known as steam-assisted gravity drainage to extract bitumen—a very viscous oil, taking advantage of the pore-scale quantification of fluid dynamics at relevant reservoir conditions and pore sizes. It is found that the characteristic size of oil-in-water emulsions generated is reduced from 150 to 6 μm and the corresponding recovery effectiveness is enhanced by 50% with the additive.

3.3. CO_2 sequestration

Four mechanisms have been proposed for CO_2 sequestration in saline aquifers: structural and hydrodynamic capture due to the density difference between the liquid and CO_2, residual capture during the formation of the porous spaces, the solubility capture owing to the

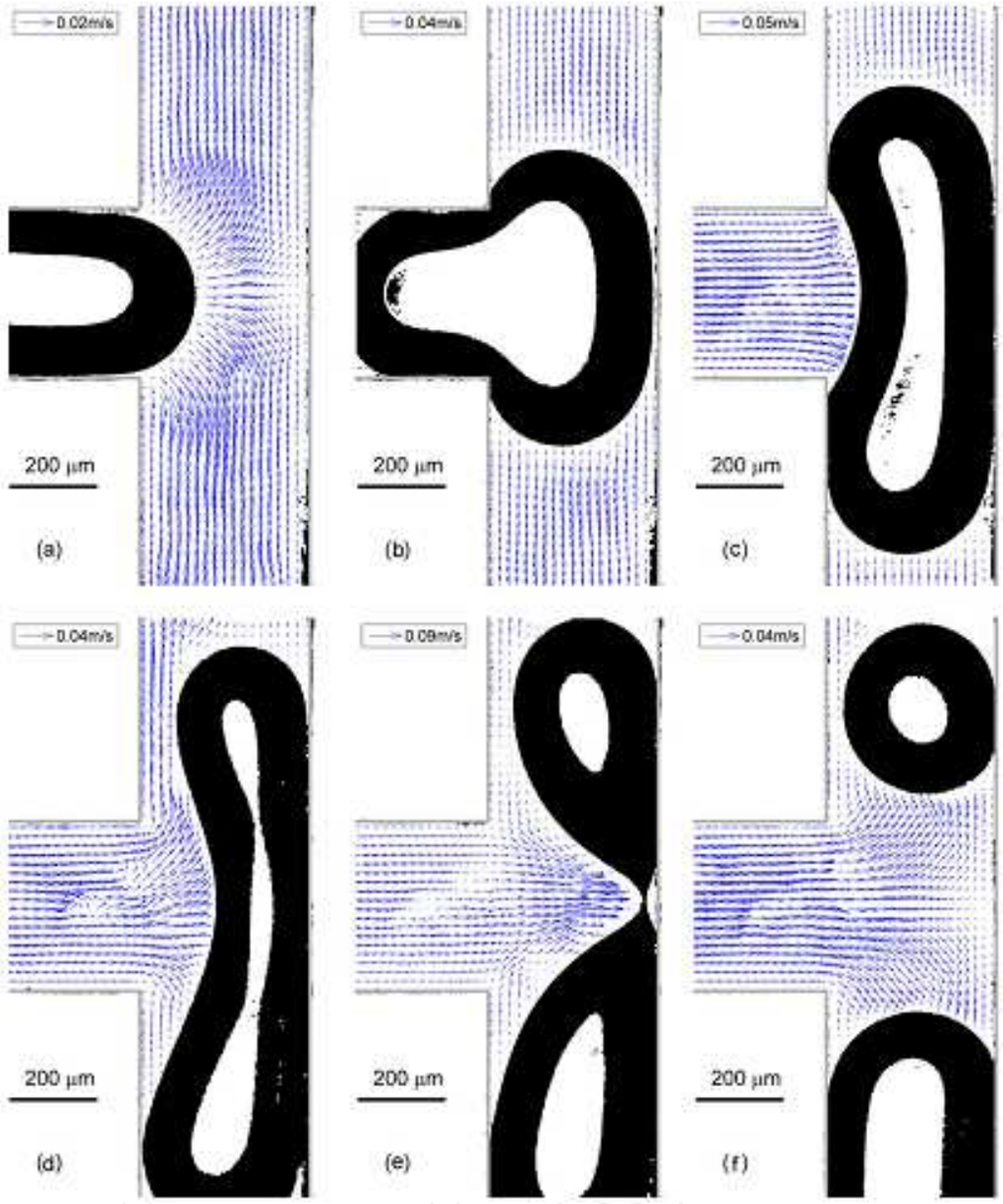

Figure 4. Velocity fields in the liquid phase around a breaking bubble at a T-junction with the help of micro-PIV. Reprinted from Fu et al. (2014). (Reproduced with permission. Copyright John Wiley and Sons, 2014) (Fu et al. [4]) http://dx.doi.org/10.1002/aic.14377.

dissolvedCO_2 in the liquid phase, and mineral capture due to the stable carbonate formed by the reaction of CO_2 and rock minerals [40]. In general, low-pressure foam micromodel studies physically show the effect of foam within the porous media. To highlight chemical interactions with the oil phase requires all phases to be at reservoir pressure. Ma et al. [55] used a micromodel to investigate the sweep efficiency of the surfactant CO_2 foam in a heterogeneous network without oil at ambient conditions. Kumar Gunda et al. [56] designed a "reservoir-on-a-chip" to represent the pore structure of a naturally oil-bearing reservoir rock to perform conventional water-flooding experiments, and observed in real time the fluid-fluid interface

http://dx.doi.org/10.5772/64284

structure at the junctions of the porous media (Figure 5). The fluid-fluid interface is found to be trapped at some junctions by capillary trapping. Datta et al. [57] constructed velocity distributions in a fluid flow in a three-dimensional porous media by using the confocal microscopy, and they found that the velocity magnitudes and the velocity components both along and transvers to the imposed flow direction were distributed exponentially. They also observed that the pore-scale correlations in the flow were predominated by the geometry of the media, which suggested that the fluid flow through the pore space was not completely random despite the considerable complexity of it. Wu et al. [58] studied the effect of the wettability of the channel and the morphology of the network on the fluid flow for the displacement of oil by water in porous media with a microfluidic model. The former affects the structure of the water phase, while the latter determines the residual oil saturation. The networks used in this study were composed of about 600 grains separated by a highly connected network of channels with an overall porosity of 0.11–0.20. The findings suggested that the morphology of the complex network resulted in a complex flow behavior that was difficult to predict by solely on porosity, and they provided a versatile tool on the study of visualized multiphase flow behavior and displacement mechanism in porous media at the microscale, nanoscale, and pore scale.

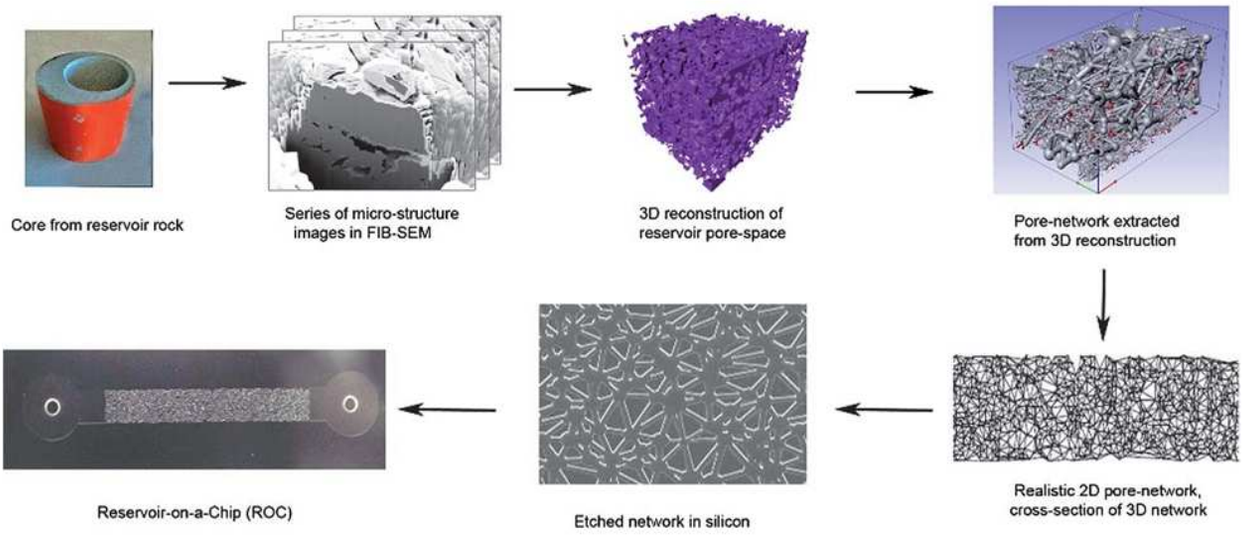

Figure 5. The conceptual map for "reservoir-on-a-chip." Reproduced from Kumar Gunda et al. [56] with permission of The Royal Society of Chemistry. http://dx.doi.org/10.1039/C1LC20556K

Several studies show that the dynamics of the fluid-fluid interface at the microscale is influenced by the morphology and wettability of the microchannels in porous space. Berejnov et al. [59] constructed a lab-on-a-chip to study the effect of the wettability of microchannels on the selectivity and percolation patterns of multiphase flow in networks with 5000 channels at pore scale. Murison et al. [60] found that additional dissipation at small extension can be caused by the contact line pinning of gas beads for a dense packing. More attention should be paid to the effects of morphology of porous media and wettability on multiphase flow in porous spaces.

To overcome the difference between the material used for typical microfluidic devices (glass, silicone, and PDMS) and the real rock for CO_2 flooding and sequestration, Song et al. [61] presented a real-rock micromodel made in a naturally mineral substrate as shown in Figure 6, to directly study the multiphase flow behavior and multicomponent interactions in real time. They demonstrated the dissolution of carbonate rock with time resulted by hydrochloric acid flow relevant to acidizing processes for reservoir stimulations. Flow and crystal orientation-directed preferential dissolution was observed. This work paves the way for future applications of real-rock microfluidics, highlighting processes in the subsurface, to study the fundamental fluid-rock interactions and examine the effect of industrially relevant injection fluids on CO_2 storage in saline aquifers.

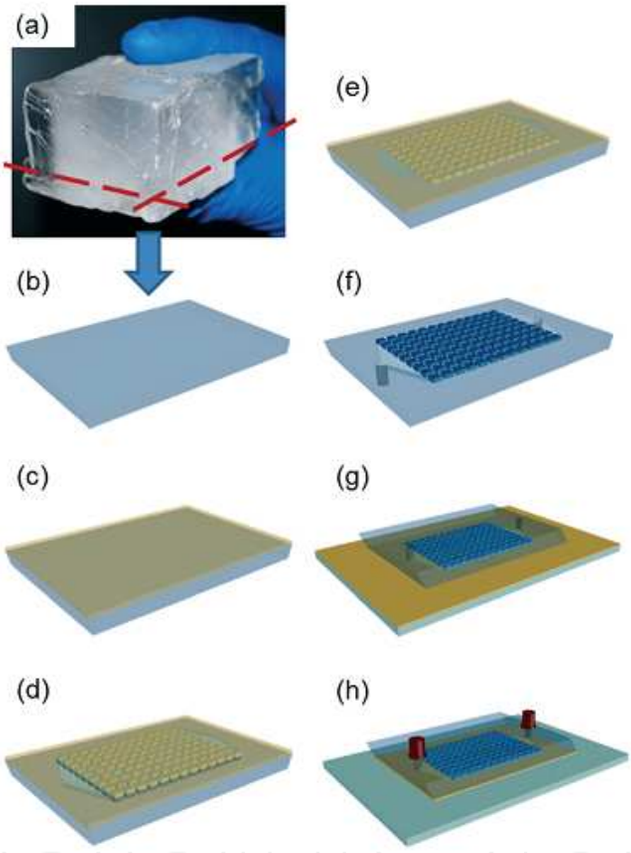

Figure 6. Fabrication of the microfluidic devices made in natural calcite material. Reproduced from Song et al. [61] with permission of The Royal Society of Chemistry. http://dx.doi.org/10.1039/C4LC00608A

In general, low-pressure foam micromodel studies demonstrate the effect of foam as a physical structure within the porous media. To include representative chemical interactions with the oil phase requires all phases to be at reservoir pressure. The microfluidic technique is also tested for high pressure CO_2 injection, supercritical CO_2 injection, CO_2-surfactant injection, and low-pressure air-surfactant injection [31]. Nguyen et al. [62] provided a microcore method to study the porosity and permeability changes for pore-scale analysis of superficial CO_2 reactive transport in saline aquifers at reservoir temperature and pressure conditions of 8.4 MPa and

40°C. Kim et al. [63] presented another lab-on-a-chip approach to understand the process of salt precipitation during CO_2 sequestration at pore scale. The dynamics of flow, evaporation, and salt formation within porous media could be observed in the complex networks consisting of microchannels with pore size distributions relevant to native porous media. Salt precipitation happens streamwise with a speed equivalent to 2% of the CO_2 velocity. The salt formation mechanism could also be identified at the pore scale using this method: large bulk crystals forming early in the trapped brine phases on the order of the pore size; and polycrystalline aggregated structures forming late in the evaporation process on a wide range of length scale. These findings can be used to explore the blockage phenomenon and well bore dry-out strategy. Nguyen et al. [64] evaluated nanoparticle CO_2 foam stability and EOR efficiency by using a micromodel approach, providing a quantitative measurement of bubble size and coalescence dynamics. In comparison to other similar cases with CO_2 gas, the nanoparticle-stabilized CO_2 foam showed a three-fold increase in oil recovery attributed to the role of the physical pore-scale bubble structures, which are rendered very stable in the presence of nanoparticles.

4. Conclusions and perspectives

In conclusion, microfluidic technique is a promising tool for CO_2 capture, sequestration, and application. To further take advantage of this new technique, several challenges, needs, and future directions should be highlighted. The detailed fluid dynamics for multiphase flow in single microchannels, single-stage microfluidic divergences and doublet microchannels, and multistage microfluidic divergences and network microchannels need to be explored. The fascinating fluid dynamics at fluid-fluid interface involving surface tension at microscale is still challenging. The stability and non-stability of the fluid-fluid interface at microchannels and networks need to be emphasized to gain insights into the mechanism for fluid flow in porous media for the CO_2 capture, sequestration, and applications. For example, the breakup and nonbreakup of the fluid-fluid interface and the trapping and releasing of bubbles in microchannels should be explored. Studies on the effects of the gas and liquid flow rate, pressure, temperature, the viscosity and surface tension of the liquid phase, the wettability of the channel wall, the geometry and size of microchannels, and the structural morphology of multistage microchannels on the dynamical evolution of the fluid-fluid interface should be explored.

It is urgent to conduct studies on CO_2 utilization in line with the pressure, temperature, and materials for porous media in practical application at the microreactor scale and pore scale. The most challenging problem is how to evaluate and manipulate the fluid-fluid interface for both immiscible and miscible systems at the microreactor scale and pore scale. Many of pore-scale phenomena need to be explored, including the behavior of the wetting films, the movement of contact lines and dynamic contact angles, the stability of capillary bridges, the dynamic instability of nonwetting fluid, the propagation of fluid-fluid interface, even the phase transitions during multiphase flowing, the heat and mass transfer across interfaces, and many others.

Acknowledgements

The financial supports for this project from the National Natural Science Foundation of China (21106093), the Research Fund for the Doctoral Program of Higher Education (20110032120010), and the Elite Scholar Program of Tianjin University are gratefully acknowledged.

Author details

Taotao Fu[1,2*]

Address all correspondence to: ttfu@tju.edu.cn

1 State Key Laboratory of Chemical Engineering, Collaborative Innovation Center of Chemical Science and Engineering, Tianjin, China

2 School of Chemical Engineering and Technology, Tianjin University, Tianjin, China

References

[1] K. S. Elvira, X. C. I. Solvas, R. C. R. Wootton, and A. J. deMello, Nature Chemistry 5, 905 (2013).

[2] V. Hessel, I. Vural Gürsel, Q. Wang, T. Noël, and J. Lang, Chemical Engineering & Technology 35, 1184 (2012).

[3] M. T. Kreutzer, F. Kapteijn, J. A. Moulijn, and J. J. Heiszwolf, Chemical Engineering Science 60, 5895 (2005).

[4] T. Fu, Y. Ma, and H. Z. Li, AIChE Journal 60, 1920 (2014).

[5] M. J. Fuerstman, A. Lai, M. E. Thurlow, S. S. Shevkoplyas, H. A. Stone, and G. M. Whitesides, Lab on a Chip 7, 1479 (2007).

[6] F. P. Bretherton, Journal of Fluid Mechanics 10, 166 (1961).

[7] J. Ratulowski and H.-C. Chang, Physics of Fluids A: Fluid Dynamics 1, 1642 (1989).

[8] M. T. Kreutzer, F. Kapteijn, J. A. Moulijn, C. R. Kleijn, and J. J. Heiszwolf, AIChE Journal 51, 2428 (2005).

[9] W. B. Kolb and R. L. Cerro, Physics of Fluids A: Fluid Dynamics 5, 1549 (1993).

[10] H. Wong, C. J. Radke, and S. Morris, Journal of Fluid Mechanics 292, 95 (1995).

[11] J. Yue, G. Chen, Q. Yuan, L. Luo, and Y. Gonthier, Chemical Engineering Science 62, 2096 (2007).

[12] P. Sobieszuk, R. Pohorecki, P. Cyganski, M. Kraut, and F. Olschewski, Chemical Engineering Journal 164, 10 (2010).

[13] G. Bercic and A. Pintar, Chemical Engineering Science 52, 3709 (1997).

[14] J. M. van Baten and R. Krishna, Chemical Engineering Science 59, 2535 (2004).

[15] J. M. van Baten and R. Krishna, Chemical Engineering Science 60, 1117 (2005).

[16] C. O. Vandu, H. Liu, and R. Krishna, Chemical Engineering Science 60, 6430 (2005).

[17] J. Yue, L. Luo, Y. Gonthier, G. Chen, and Q. Yuan, Chemical Engineering Science 64, 3697 (2009).

[18] J. C. Jepsen, AIChE Journal 16, 705 (1970).

[19] D. Eskin and F. Mostowfi, International Journal of Heat and Fluid Flow 33, 147 (2012).

[20] N. Shao, A. Gavriilidis, and P. Angeli, Chemical Engineering Journal 160, 873 (2010).

[21] P. Sobieszuk, R. Pohorecki, P. Cyganski, and J. Grzelka, Chemical Engineering Science 66, 6048 (2011).

[22] M. Ichiyanagi, I. Tsutsui, Y. Kakinuma, Y. Sato, and K. Hishida, International Journal of Heat and Mass Transfer 55, 2872 (2012).

[23] J. Tan, Y. C. Lu, J. H. Xu, and G. S. Luo, Chemical Engineering Journal 185-186, 314 (2012).

[24] J. Tan, Y. C. Lu, J. H. Xu, and G. S. Luo, Chemical Engineering Journal 181-182, 229 (2012).

[25] R. Sun and T. Cubaud, Lab on a Chip 11, 2924 (2011).

[26] C. Zhu, C. Li, X. Gao, Y. Ma, and D. Liu, International Journal of Heat and Mass Transfer 73, 492 (2014).

[27] C. Yao, Z. Dong, Y. Zhao, and G. Chen, Chemical Engineering Science 112, 15 (2014).

[28] L. Yang, J. Tan, K. Wang, and G. Luo, Chemical Engineering Science 109, 306 (2014).

[29] Y. Su, Y. Zhao, F. Jiao, G. Chen, and Q. Yuan, AIChE Journal 57, 1409 (2011).

[30] Y. Su, G. Chen, Y. Zhao, and Q. Yuan, AIChE Journal 55, 1948 (2009).

[31] D. Sinton, Lab on a Chip 14, 3127 (2014).

[32] A. Sell, H. Fadaei, M. Kim, and D. Sinton, Environmental Science & Technology 47, 71 (2013).

[33] H. Fadaei, B. Scarff, and D. Sinton, Energy & Fuels 25, 4829 (2011).

[34] S. Lefortier, P. Hamersma, A. Bardow, and M. T. Kreutzer, Lab on a Chip 12, 3387 (2012).

[35] M. Abolhasani, M. Singh, E. Kumacheva, and A. Gunther, Lab on a Chip 12, 1611 (2012).

[36] W. Li, K. Liu, R. Simms, J. Greener, D. Jagadeesan, S. Pinto, A. Gunther, and E. Kumacheva, Journal of the American Chemical Society 134, 3127 (2012).

[37] E. Tumarkin, Z. Nie, J. I. Park, M. Abolhasani, J. Greener, B. Sherwood-Lollar, A. Gunther, and E. Kumacheva, Lab on a Chip 11, 3545 (2011).

[38] E. Tumarkin, J. I. Park, Z. Nie, and E. Kumacheva, Chemical Communications 47 (2011).

[39] J. I. Park, Z. Nie, A. Kumachev, and E. Kumacheva, Soft Matter 6, 630 (2010).

[40] D. P. Schrag, Science 315, 812 (2007).

[41] G. Dawson, S. Lee, and A. Juel, Journal of Fluid Mechanics 722, 437 (2013).

[42] G. I. Taylor, Journal of Fluid Mechanics 10, 161 (1961).

[43] G. M. Homsy, Annual Review of Fluid Mechanics 19, 271 (1987).

[44] H. E. Huppert and J. A. Neufeld, Annual Review of Fluid Mechanics 46, 255 (2014).

[45] U. Oxaal, M. Murat, F. Boger, A. Aharony, J. Feder, and T. Jossang, Nature 329, 32 (1987).

[46] T. T. Al-Housseiny, J. Hernandez, and H. A. Stone, Physics of Fluids 26, 042110 (2014).

[47] T. T. Al-Housseiny and H. A. Stone, Physics of Fluids 25, 092102 (2013).

[48] T. T. Al-Housseiny, P. A. Tsai, and H. A. Stone, Nat Phys 8, 747 (2012).

[49] R. Lenormand, C. Zarcone, and A. Sarr, Journal of Fluid Mechanics 135, 337 (1983).

[50] T. T. Al-Housseiny, I. C. Christov, and H. A. Stone, Physical Review Letters 111, 034502 (2013).

[51] T. Fu, Y. Ma, D. Funfschilling, and H. Z. Li, Chemical Engineering Science 66, 4184 (2011).

[52] X. Wang, C. Zhu, T. Fu, and Y. Ma, AIChE Journal 61, 1081 (2015).

[53] X. Wang, C. Zhu, T. Fu, and Y. Ma, Chemical Engineering Science 111, 244 (2014).

[54] T. W. de Haas, H. Fadaei, U. Guerrero, and D. Sinton, Lab on a Chip 13, 3832 (2013).

http://dx.doi.org/10.5772/64284

[55] K. Ma, R. Liontas, C. A. Conn, G. J. Hirasaki, and S. L. Biswal, Soft Matter 8, 10669 (2012).

[56] N. S. Kumar Gunda, B. Bera, N. K. Karadimitriou, S. K. Mitra, and S. M. Hassanizadeh, Lab on a Chip 11, 3785 (2011).

[57] S. S. Datta, H. Chiang, T. S. Ramakrishnan, and D. A. Weitz, Physical Review Letters 111, 064501 (2013).

[58] M. Wu, F. Xiao, R. M. Johnson-Paben, S. T. Retterer, X. Yin, and K. B. Neeves, Lab on a Chip 12, 253 (2012).

[59] V. Berejnov, N. Djilali, and D. Sinton, Lab on a Chip 8, 689 (2008).

[60] J. Murison, B. Semin, J.-C. Baret, S. Herminghaus, M. Schröter, and M. Brinkmann, Physical Review Applied 2, 034002 (2014).

[61] W. Song, T. W. de Haas, H. Fadaei, and D. Sinton, Lab on a Chip 14, 4382 (2014).

[62] P. Nguyen, H. Fadaei, and D. Sinton, Journal of Fluids Engineering 135, 021203 (2013).

[63] M. Kim, A. Sell, and D. Sinton, Lab on a Chip 13, 2508 (2013).

[64] P. Nguyen, H. Fadaei, and D. Sinton, Energy & Fuels 28, 6221 (2014).

IntechOpen